ACS NANO

www.acsnano.org

ARTICLE

Optimizing Charge Injection across Transition Metal Dichalcogenide Heterojunctions: Theory and Experiment

Jie Guan,[†] Hsun-Jen Chuang,[‡] Zhixian Zhou,[‡] and David Tománek*,[†]

[†]Physics and Astronomy Department, Michigan State University, East Lansing, Michigan 48824, United States

[‡]Physics and Astronomy Department, Wayne State University, Detroit, Michigan 48201, United States

Supporting Information

ABSTRACT: **In search of an improved strategy to form low-resistance contacts to semiconducting transition metal dichalcogenides, we combine *ab initio* density functional electronic structure calculations for an $NbSe_2/WSe_2$ interface with quantum transport measurements of the corresponding heterojunction between a few-layer WSe_2 semiconductor and a metallic $NbSe_2$ layer. Our theoretical results suggest that, besides a rigid band shift associated with charge transfer, the presence of $NbSe_2$ does not modify the electronic structure of WSe_2. Since the two transition metal dichalcogenides are structurally similar and display only a small lattice mismatch, their heterojunction can efficiently transfer charge across the interface. These findings are supported by transport measurements for WSe_2 field-effect transistors with $NbSe_2$ contacts, which exhibit nearly ohmic behavior and phonon-limited mobility in the hole channel, indicating that the contacts to WSe_2 are highly transparent.**

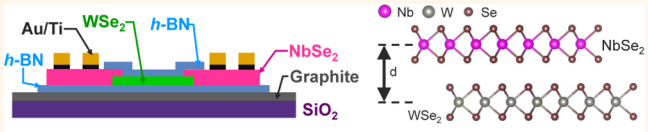

WSe_2 field-effect transistor with $NbSe_2$ leads in side view. Schematic structure of the device (left) and an atomic-model representation of the $WSe_2/NbSe_2$ interface (right).

KEYWORDS: *transition metal dichalcogenides, contacts, heterojunctions, ab initio calculations, electronic structure*

Since mechanically exfoliated ultrathin niobium diselenide[1] ($NbSe_2$) has displayed superconducting behavior and single-layer molybdenum disulfide[2] (MoS_2) has been identified as a direct-gap semiconductor[3] and used in a field-effect transistor,[4] the family of layered transition metal dichalcogenide (TMD) materials has attracted much attention as promising candidates for two-dimensional (2D) electronics and optoelectronics applications.[5,6] Even though much effort has been spent to fabricate high-performance devices, the success has been limited by lack of a viable strategy to form low-resistance ohmic contacts between TMDs and electrodes.[7−10] The local doping method used at silicon−metal interfaces in traditional three-dimensional (3D) Si devices can not be replicated in 2D systems.[11−16] In TMDs contacted by a metal, carrier injection across the interface is typically limited by significant Schottky barriers. This effect can be partly mitigated by using metals with a work function close to the conduction band minimum (CBM) or valence band maximum (VBM), which lowers the Schottky barrier height (SBH) and thus decreases the contact resistance.[17−20] Still, the complex Fermi level pinning at the electrode-semiconductor interface makes it even harder to achieve ohmic contacts.[21−25] Other strategies to reduce the contact resistance, including attempts to fabricate in-layer junctions by phase engineering,[26,27] 2D/2D interlayer junctions with weak Fermi level pinning,[28] use of doped graphene,[29−32] doped TMDs,[33] or inserting hexagonal boron nitride (hBN) at the metal-TMD interface,[34] have been met with mixed success.

Our choice of metallic TMDs as drain/source contacts is largely motivated by the successful demonstration of graphene as a contact material for achieving low-resistance contacts to semiconducting TMDs.[29,31,35−37] However, the atomic thickness and rather low sheet carrier density in graphene also introduce a relatively high effective contact resistance comprised of the graphene sheet resistance and the graphene/metal contact resistance. A good strategy to further reduce the effective contact resistance in TMD field-effect transistors (FETs) is to replace graphene as contact material by 2D metallic TMDs with substantially lower sheet resistance and fewer interface states due to the lack of dangling bonds.

Here we propose to use metallic TMDs as drain/source contacts as an alternative to previous contacting strategies that may provide low-resistance contacts to semiconducting TMDs. We combine *ab initio* density functional electronic structure calculations for an $NbSe_2/WSe_2$ interface with quantum transport measurements of the corresponding heterojunction between a few-layer WSe_2 semiconductor and a metallic $NbSe_2$ layer. Our theoretical results suggest that, besides a small rigid band shift associated with charge transfer, the presence of

Received: January 13, 2017
Accepted: March 20, 2017
Published: March 20, 2017

DOI: 10.1021/acsnano.7b00285
ACS Nano 2017, 11, 3904−3910

$NbSe_2$ does not modify the electronic structure of WSe_2. Since the two transition metal dichalcogenides are structurally similar and display only a small lattice mismatch, their heterojunction gives rise to only a small tunnel barrier so that charge can be injected efficiently across the interface. These findings are supported by transport measurements for WSe_2 field-effect transistors (FETs) with $NbSe_2$ contacts and a graphite gate, which exhibit nearly ohmic behavior and phonon-limited mobility in the hole channel, indicating that the contacts to WSe_2 are highly transparent.

RESULTS AND DISCUSSION

We first optimized the bulk structure of $NbSe_2$ and WSe_2 in the stable 2H phase and show our results in Figure 2a,b. Results of our DFT-optB86b-vdW calculations show that the AB layer stacking is energetically favorable to the AA stacking in both systems. For bulk $NbSe_2$, we found that our calculated in-plane lattice constant a_{theor} = 3.46 Å lies close to the observed value[38] a_{expt} = 3.44 Å. Similarly, the calculated out-of-plane lattice constant c_{theor} = 12.74 Å, extending over two interlayer distances, lies close to the observed value[38] c_{expt} = 12.48 Å. Also for bulk WSe_2, we obtained very good agreement with the experiment[39] between a_{theor} = 3.30 Å and a_{expt} = 3.28 Å for the in-layer lattice constant and c_{theor} = 13.10 Å and c_{expt} = 12.96 Å for the out-of-plane lattice constant. We notice that the in-layer lattice constant of $NbSe_2$ is only 5% larger than that of WSe_2 in the bulk, suggesting the likelihood of epitaxial stacking especially in few-layer systems.

We also found the AB stacking sequence to be preferred for the 2H-$NbSe_2$/2H-WSe_2 bilayer, depicted in Figure 1. The

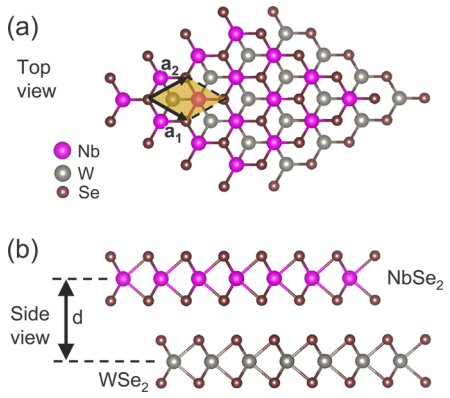

Figure 1. (Color online) Ball-and-stick model of an AB-stacked $NbSe_2$/WSe_2 bilayer in (a) top view and (b) side view. The unit cell is indicated by yellow shading in the top view. a_1 and a_2 are the lattice vectors spanning the 2D lattice and d is the interlayer distance.

bilayer forms a honeycomb lattice with 6 atoms per unit cell, 3 of which are in the $NbSe_2$ and the other 3 in the WSe_2 layer. As seen in Figure 2c, the optimum in-layer lattice constant a_{theor} = 3.37 Å lies in-between the values for the individual bulk components. Also, as seen in Figure 2d, the value d_{theor} = 6.41 Å for the optimum interlayer distance, lies in-between the corresponding values in bulk $NbSe_2$ and WSe_2. The binding energy of the two layers is 0.19 eV per unit cell, based on DFT-optB86b-vdW, indicates that the interlayer coupling is weak.

The parabola fits of energy differences ΔE, shown by the dashed lines in Figure 2, indicate harmonic behavior of the bulk and bilayer structures within ≈10% of the optimum lattice constant a or interlayer distance d.

Electronic band structure results for the $NbSe_2$/WSe_2 bilayer and its monolayer components are shown in Figure 3. As seen in Figure 3a, the $NbSe_2$/WSe_2 bilayer is metallic. To interpret the band structure of the bilayer, we calculated separately the band structure of isolated $NbSe_2$ and WSe_2 monolayers and displayed it in Figure 3b. These results indicate that the $NbSe_2$ monolayer is metallic, whereas the WSe_2 monolayer is semiconducting with a direct gap of about 1.35 eV at the K point. Even though the absolute value of the band gap is typically underestimated in DFT calculations, the dispersion of individual bands is usually in good agreement with more accurate self-energy calculations. We found that individual bands in isolated $NbSe_2$ and WSe_2 monolayers in Figure 3b can be identified in the band structure of the bilayer. To prove this point, we superposed the band structure of the two constituents, shifting the bands of WSe_2 rigidly up by 0.293 eV in Figure 3b, and present the resulting band structure in Figure 3c, along with the bilayer result of Figure 3a. The agreement between the band structure of the bilayer and the superposition of monolayers is near-perfect, suggesting the applicability of a rigid-band model in this system. Our finding that there is nearly no band rehybridization, but only a minor band realignment at the interface of $NbSe_2$ and WSe_2 monolayers also holds for WSe_2 multilayers with a narrower and indirect band gap.

As mentioned earlier, $NbSe_2$ is compressed by < 3% and WSe_2 stretched by < 3% in the bilayer as a result of the difference between the lattice constants. We found that these modest structural changes have a negligible effect on the electronic band structure.

To better characterize the $NbSe_2$/WSe_2 interface, we calculated the charge density difference $\Delta\rho = \rho_{tot}(\text{bilayer}) - \sum\rho_{tot}(\text{monolayers})$ associated with the assembly of the bilayer from isolated monolayers using a supercell with the lattice constant c = 24.0 Å, about four times the interlayer distance. This charge density difference is visualized by contour plots in Figure 4a. We find that the charge redistribution is very small, with electrons transferring mainly from the WSe_2 layer to the interlayer region and to the $NbSe_2$ layer. To further elucidate the charge redistribution, we averaged the charge density difference in planes with z = const. that are parallel to the $NbSe_2$ and WSe_2 layers. The averaged quantity $\langle\Delta\rho(z/c)\rangle$, shown by the solid line in Figure 4b, displays many oscillations even in individual TMD layers. To better understand the net charge flow, we convoluted the raw data by a Gaussian with a full-width at half-maximum of 0.17. The resulting function, displayed by the blue dashed line in Figure 4b, indicates a very small net flow of electrons from WSe_2 and the interface to the $NbSe_2$ layer. This result is consistent with the upward shift of WSe_2 bands discussed in relation to Figure 3c and also a previous report for the VS_2/MoS_2 bilayer system.[28] As a more quantitative measure of the charge redistribution, we performed the Bader charge analysis[40−43] in the $NbSe_2$/WSe_2 bilayer and found that 0.017 electrons per unit cell have been transferred from the WSe_2 to the $NbSe_2$ layer upon forming the interface.

Since charge injection across the interface is limited by potential energy barriers, which act as tunnel or Schottky barriers, we also investigated the local electrostatic potential V in the whole $NbSe_2$/WSe_2 interface region. To facilitate the interpretation, we averaged V in z = const. planes, similar to the way we averaged the charge density difference $\Delta\rho(z/c)$ in

DOI: 10.1021/acsnano.7b00285
ACS Nano 2017, 11, 3904−3910

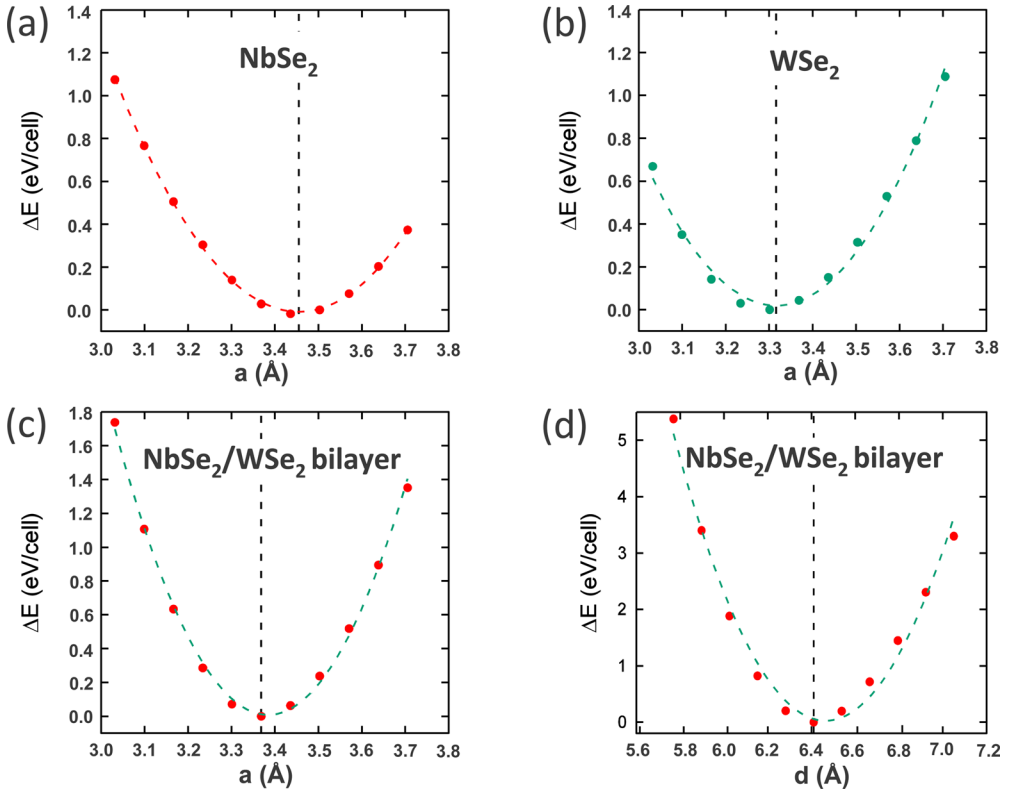

Figure 2. (Color online) Energy change ΔE per unit cell as a function of the lattice constant $a = |a_1| = |a_2|$ in (a) bulk $NbSe_2$ and (b) bulk WSe_2 in the stable 2H phase. ΔE per unit cell of the AB-stacked $NbSe_2/WSe_2$ bilayer as a function of (c) the lattice constant a and (d) the interlayer distance d. The dashed lines show parabola fits.

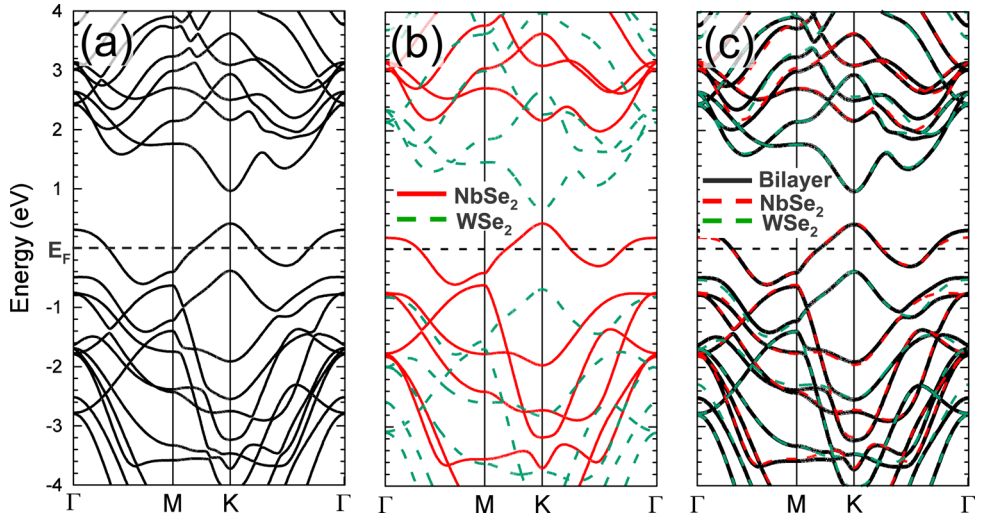

Figure 3. (Color online) (a) Electronic band structure of a $NbSe_2/WSe_2$ bilayer. (b) Superposition of the electronic band structure of isolated monolayers of $NbSe_2$ (solid red lines) and WSe_2 (dashed green lines). (c) Superposition of the WSe_2 bands in panel (b), shifted rigidly up by 0.293 eV, and the $NbSe_2$ bands in panel (b). This combined band structure is superposed to that of the $NbSe_2/WSe_2$ bilayer of panel (a).

Figure 4b. The corresponding results for $\langle V(z/c)\rangle$ are presented in Figure 4c. The difference between the electrostatic potential in the vacuum region and at the Fermi level, given by $V_{vacuum} - E_F \approx 5.6$ eV, corresponds to the work function. We also observe a narrow tunnel barrier characterized by $\Delta(z) \approx 1.8$ Å and $\Delta V \approx 4.5$ eV when measured from the Fermi level, resulting in a high tunneling probability across the interface, translating into high contact transparency.[18]

As a counterpart of the theoretical study, we have fabricated few-layer WSe_2 FETs with $NbSe_2$ drain/source contacts using van der Waals assembly. Our experimental results are summarized in Figure 5. Figure 5a illustrates schematically a few-layer WSe_2 FET with $NbSe_2$ drain and source contacts. The WSe_2 channel is placed on top of an hBN/graphite stack and is passivated by another hBN thin crystal from the top. Graphite is used as a gate electrode. These devices exhibit highly asymmetric ambipolar behavior with significantly higher hole than electron current, indicating that the Fermi level of $NbSe_2$ is aligned much closer with the VBM than the CBM of WSe_2. This is consistent with our band structure results for the

DOI: 10.1021/acsnano.7b00285
ACS Nano 2017, 11, 3904−3910

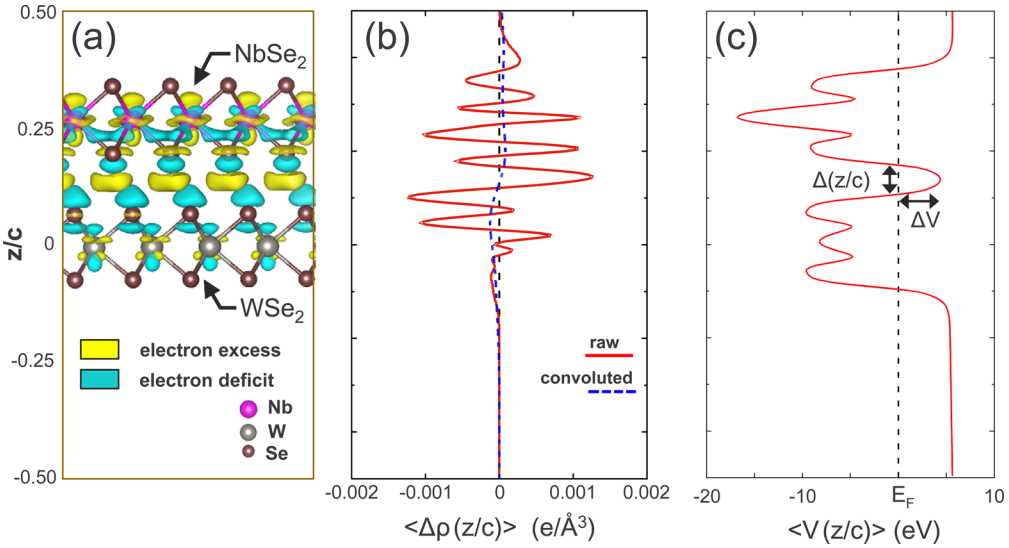

Figure 4. (Color online) Electronic structure changes associated with assembling the $NbSe_2/WSe_2$ bilayer from isolated monolayers. (a) Charge density difference $\Delta\rho = \rho(NbSe_2/WSe_2) - \rho(NbSe_2) - \rho(WSe_2)$. $\Delta\rho$ is shown by isosurfaces bounding regions of electron excess at $+2.5 \times 10^{-4}$ e/Å^3 (yellow) and electron deficiency at -2.5×10^{-4} e/Å^3 (blue). (b) $\langle\Delta\rho(z/c)\rangle$ averaged across the $x - y$ plane of the layers. The raw data, shown by the red solid line, and their convolution by a Gaussian with a full-width at half-maximum $\Delta(z/c) = 0.17$, shown by the blue dashed line. (c) Electrostatic potential $\langle V(z/c)\rangle$ averaged across the $x - y$ plane of the layers. z/c indicates the relative position of the plane within the unit cell with $c = 24.0$ Å.

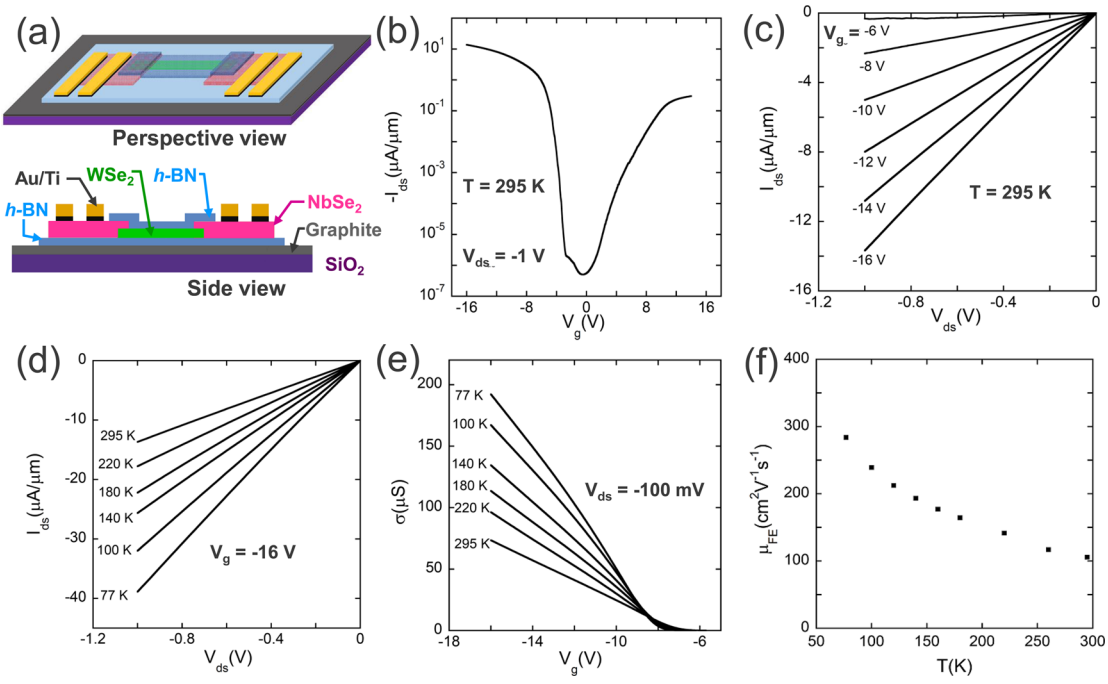

Figure 5. (Color online) Design and characteristics of a few-layer WSe_2 FET with $NbSe_2$ contacts. (a) Schematic illustration of the WSe_2 device with $NbSe_2$ drain/source contacts and a graphite gate. The channel has been an encapsulated in hBN. (b) Room-temperature $I_{ds}-V_g$ transfer characteristics of a WSe_2 FET exhibiting asymmetric ambipolar behavior with an on/off ratio of 10^7 for holes and 10^5 for electrons. The WSe_2 channel is ≈5.5 nm thick, ≈5.5 μm long, and ≈2.6 μm wide. (c, d) Linearity of the $I_{ds}-V_{ds}$ output characteristics of the WSe_2 device. Room-temperature measurements for gate voltages ranging between $V_g = -16$ V and -6 V (c) are compared to measurements at $V_g = -16$ V in the temperature range from $T = 77$ to 295 K (d). Both sets of measurements indicate that contacts for the hole channel are near-ohmic. (e) Temperature-dependent two-terminal conductivity σ of the WSe_2 device as a function of gate voltage at $V_{ds} = -100$ mV. (f) Two-terminal measurements of the field-effect hole mobility μ_{FE} of the WSe_2 device as a function of temperature. Observed μ_{FE} values increase from 106 to 283 cm^{2}V^{-1}s^{-1} as the temperature decreases from 295 to 77 K.

$NbSe_2/WSe_2$ bilayer shown in Figure 3. As mentioned earlier, few-layer WSe_2 used in the experimental study has a narrower band gap than a monolayer and will incur a smaller rigid upshift of its bands.

Our observations suggest that we have achieved near-ohmic contacts for the hole channel. Variable temperature electrical measurements performed on WSe_2 FETs with $NbSe_2$ contacts reveal that as the temperature decreases from room temper-

DOI: 10.1021/acsnano.7b00285
ACS Nano 2017, 11, 3904−3910

ature to 77 K, the extrinsic two-terminal field-effect mobility increases from ≈107 to ≈286 $cm^2V^{-1}s^{-1}$, indicating that the mobility of our $NbSe_2$-contacted WSe_2 devices is limited by the phonons in the channel and not by the contacts.

The transfer curve of a typical hBN-encapsulated WSe_2 FET with $NbSe_2$ drain and source contacts and a graphite back gate is reproduced in Figure 5b. The few-layer WSe_2 device is ≈5.5 nm thick and exhibits a highly asymmetric ambipolar behavior, with an on/off ratio of 10^7 for holes and of 10^5 for electrons at a drain-source voltage of −1 V. As shown in Figure S2 in the Supporting Information, the on-state hole current is about 2 orders of magnitude higher than in our few-layer WSe_2 devices with conventional Ti/Au contacts, suggesting that 2D $NbSe_2$ is superior to conventional 3D metals as a contact material.

A gate overdrive voltage, when applied to the device, is defined as $V_{Drive} = |V_g - V_{min}|$, where V_g is the applied gate voltage and V_{min} is the gate voltage used to obtain the current minimum. Applying comparable values of gate overdrive voltages for electron and hole injection is expected to cause a similar degree of band bending. Consequently, observing a nearly 2 orders of magnitude higher on-current in the hole channel than in the electron channel suggests that the Fermi level of $NbSe_2$ contacts is aligned much closer to the VBM than to the CBM of WSe_2. We thus conclude that the tunnel or Schottky barrier height is much lower for the hole channel than for the electron channel.[7]

Next, we focus on the hole channel of the device. As shown in Figure 5c, the output characteristics of the WSe_2 device at room temperature are linear at all gate voltages between V_g = −16 V and −6 V. Whereas a linear $I_{ds}-V_{ds}$ characteristic usually indicates an ohmic contact, thermally assisted tunneling through a finite tunnel or Schottky barrier could also lead to linear response.[9] To shed additional light on the quality of the $NbSe_2$ contacts, we performed temperature dependent measurements and present them in Figure 5d. Indeed, these results show that the $I_{ds}-V_{ds}$ curves remain linear down to T = 77 K at a gate voltage V_g = −16 V, providing further evidence that $NbSe_2$ forms low-barrier and highly transparent contacts to the WSe_2 channel for hole injection.

It is worth pointing out that the rigid upshift of WSe_2 bands, predicted for the $NbSe_2/WSe_2$ bilayer, is expected to be significantly reduced for $NbSe_2$ in contact with few-layer WSe_2 devices due to a more gradual charge redistribution and a smaller band gap in few-layer WSe_2. Consequently, the band offset between WSe_2 in the $NbSe_2/WSe_2$ contact region and in the channel region will also be reduced. Consequently, the in-plane Schottky barrier between few-layer WSe_2 interfacing $NbSe_2$ in the contact region and the isolated WSe_2 channel will be diminished, leading to the experimentally observed ohmic behavior in $NbSe_2$-contacted few-layer WSe_2 devices.

To further demonstrate the high quality of the $NbSe_2$ contacts, we reproduce in Figure 5e the two-terminal conductivity of the same WSe_2 device at different temperatures. The two-terminal conductivity is defined by $\sigma = I_{ds}/V_{ds} \times L/W$, where L is the length and W the width of the channel. Similar to WSe_2 FETs with graphene and 2D/2D contacts, which have been reported in our previous studies,[29,33] the WSe_2 channel with $NbSe_2$ contacts also exhibits a metal−insulator transition (MIT). The on-state conductivity at V_g = −16 V increases monotonically by a factor of ≈3 as the temperature decreases from T = 295 to 77 K.

Finally, we extracted the field-effect mobility from the linear region of the conductivity curves in the metallic state at $-16\ V < V_g < -10\ V$ using the expression $\mu_{FE} = (1/C_g) \times (d\sigma/dV_g)$, where C_g is the geometric gate capacitance of a 40 nm thick hBN layer[44] with ϵ = 3.5. As shown in Figure 5f, the hole mobility for the WSe_2 device increases from ≈106 $cm^2V^{-1}s^{-1}$ to ≈283 $cm^2V^{-1}s^{-1}$ as the temperature decreases from room temperature to 77 K, strongly suggesting that the hole transport in the device channel is limited by phonons and not by contacts.[29,45−47] The two-terminal field-effect mobility in our $NbSe_2$-contacted WSe_2 devices is significantly higher than what has been reported for few-layer WSe_2 devices with platinum bottom contacts.[24] The weaker-than-expected temperature dependence of the two-terminal field-effect mobility could be attributed to the presence of a finite contact resistance. The limiting effect of the contact resistance on the current starts playing an increasing role as the channel resistance decreases with decreasing temperature.

Our study indicates that Schottky/tunnel barriers between metallic and semiconducting TMDs are fundamentally different from conventional metal−semiconductor Schottky barriers for the following two important reasons. First, the formation of interface states is suppressed in TMD heterojunctions due to the lack of dangling bonds on TMD surfaces, similar to what is known about graphene/TMD junctions. Second, an abrupt potential drop, rather than a relatively thick depletion layer, forms across the "van der Waals gap" of TMD heterojunctions. As a result of these differences, Fermi level pinning is expected to be significantly reduced at the interface between metallic and semiconducting TMDs.

Our findings for optimizing contacts to WSe_2 as channel material can be generally applied to also other TMD semiconductors, including MoS_2, TcS_2, and $TcSe_2$, which have been proposed for FETs applications.[33,48] More recently, $NbSe_2$ has also been used as a *p*-type contact to WSe_2, but the contact quality and observed hole mobility were below our present results.[49]

It is also worth pointing out that the relative crystalline orientation between the WSe_2 channel and the $NbSe_2$ contact layer has not been optimized and is random in our devices. Further improvement of the contact quality is expected by optimizing the stacking orientation in $WSe_2/NbSe_2$ junctions.

CONCLUSIONS

In summary, we combined theoretical and experimental techniques to investigate an improved strategy to form ohmic low-resistance contacts to semiconducting TMDs. On the part of theory, we tested the potential merit of this approach using *ab initio* density functional electronic structure calculations for an $NbSe_2/WSe_2$ bilayer. Our theoretical results suggest that, besides a rigid band offset associated with a very small charge transfer, the presence of $NbSe_2$ does not modify the electronic structure of WSe_2. This basic finding remains valid also for multilayer systems. Since the two transition metal dichalcogenides are structurally similar and display only a small lattice mismatch, their heterojunction can efficiently transfer charge across the interface. These theoretical findings are supported by quantum transport measurements in a WSe_2 field-effect transistor with $NbSe_2$ contacts. We found that the heterojunction between a few-layer WSe_2 semiconductor and a metallic $NbSe_2$ layer in this device exhibits nearly ohmic behavior and phonon-limited mobility in the hole channel, indicating that the contacts to WSe_2 are highly transparent.

DOI: 10.1021/acsnano.7b00285
ACS Nano 2017, 11, 3904−3910

METHODS

Computational Techniques. We utilized *ab initio* density functional theory (DFT) as implemented in the VASP code[50−52] to obtain the optimized structure and electronic properties of the TMD systems of interest. We have applied it to WSe_2 and $NbSe_2$ monolayers, the $NbSe_2/WSe_2$ bilayer, and the corresponding bulk structures with AB stacking of layers. All 2D structures have been represented by a periodic array of slabs separated by a vacuum region in excess of 15 Å. We used projector-augmented-wave (PAW) pseudopotentials,[53] the DFT-optB86b-vdW[54,55] exchange-correlation functionals. The Brillouin zone of the primitive unit cell of the 2D structures has been sampled by an $8 \times 8 \times 1$ *k*-point grid and that of bulk structures by an $8 \times 8 \times 2$ *k*-point grid.[56] We used 500 eV as the electronic kinetic energy cutoff for the plane-wave basis and a total energy difference between subsequent self-consistency iterations below 10^{-6} eV as the criterion for reaching self-consistency. All geometries have been optimized using the conjugate-gradient method,[57] until none of the residual Hellmann−Feynman forces exceeded 10^{-2} eV/Å.

Experimental Techniques. We fabricated WSe_2 FETs with $NbSe_2$ drain/source contacts by mechanical exfoliation and van der Waals assembly of WSe_2 and $NbSe_2$ crystals using polydimethylsiloxane (PDMS) stamps as schematically shown in Figure 5a. The WSe_2 channel with $NbSe_2$ drain/source contacts has been placed onto a hBN/graphite stack previously assembled on a SiO_2 substrate and subsequently encapsulated by another hBN thin crystal from the top in order to passivate the WSe_2 channel and to minimize the oxidation of the $NbSe_2$ contacts. Subsequently, electrical leads to the metallic $NbSe_2$ layers forming the drain and source contacts and to the graphite gate were patterned by electron beam lithography followed by deposition of 5 nm Ti and 40 nm Au as leads. This yielded low-resistance ohmic contacts between the leads and $NbSe_2$, while formation of direct contacts between WSe_2 and Ti/Au has been avoided. Optical microscopy and Park-Systems XE-70 noncontact-mode atomic force microscopy were used to characterize the WSe_2, $NbSe_2$, and hBN layers. Electrical properties of the devices were measured by a Keithley 4200 semiconductor parameter analyzer in a Lakeshore Cryogenic probe station under high vacuum of 1×10^{-6} Torr.

ASSOCIATED CONTENT

Supporting Information

The Supporting Information is available free of charge on the ACS Publications website at DOI: 10.1021/acsnano.7b00285.

Optical micrographs of few-layer WSe_2 FETs with $NbSe_2$ and with conventional Ti/Au drain and source contacts, and the transfer characteristic using inferior Ti/Au contacts (PDF)

AUTHOR INFORMATION

Corresponding Author

*E-mail: tomanek@pa.msu.edu.

ORCID

David Tománek: 0000-0003-1131-4788

Notes

The authors declare no competing financial interest.

ACKNOWLEDGMENTS

J.G. and D.T. acknowledges partial support by the NSF/AFOSR EFRI 2-DARE grant number #EFMA-1433459. Z.Z. and H.J.C. acknowledge partial support by NSF grant number DMR-1308436 and the WSU Presidential Research Enhancement Award. We are grateful to David Mandrus for providing WSe_2 crystals. Computational resources have been provided by the Michigan State University High Performance Computing Center.

REFERENCES

(1) Frindt, R. F. Superconductivity in Ultrathin $NbSe_2$ Layers. *Phys. Rev. Lett.* **1972**, *28*, 299−301.

(2) Novoselov, K. S.; Jiang, D.; Schedin, F.; Booth, T. J.; Khotkevich, V. V.; Morozov, S. V.; Geim, A. K. Two-dimensional atomic crystals. *Proc. Natl. Acad. Sci. U. S. A.* **2005**, *102*, 10451−10453.

(3) Mak, K. F.; Lee, C.; Hone, J.; Shan, J.; Heinz, T. F. Atomically Thin MoS_2: A New Direct-Gap Semiconductor. *Phys. Rev. Lett.* **2010**, *105*, 136805.

(4) Radisavljevic, B.; Radenovic, A.; Brivio, J.; Giacometti, V.; Kis, A. Single-layer MoS_2 transistors. *Nat. Nanotechnol.* **2011**, *6*, 147−150.

(5) Wang, Q. H.; Kalantar-Zadeh, K.; Kis, A.; Coleman, J. N.; Strano, M. S. Electronics and optoelectronics of two-dimensional transition metal dichalcogenides. *Nat. Nanotechnol.* **2012**, *7*, 699−712.

(6) Jariwala, D.; Sangwan, V. K.; Lauhon, L. J.; Marks, T. J.; Hersam, M. C. Emerging Device Applications for Semiconducting Two-Dimensional Transition Metal Dichalcogenides. *ACS Nano* **2014**, *8*, 1102−1120.

(7) Das, S.; Appenzeller, J. WSe_2 field effect transistors with enhanced ambipolar characteristics. *Appl. Phys. Lett.* **2013**, *103*, 103501.

(8) Liu, H.; Neal, A. T.; Ye, P. D. Channel Length Scaling of MoS_2 MOSFETs. *ACS Nano* **2012**, *6*, 8563−8569.

(9) Das, S.; Chen, H.-Y.; Penumatcha, A. V.; Appenzeller, J. High Performance Multilayer MoS_2 Transistors with Scandium Contacts. *Nano Lett.* **2013**, *13*, 100−105.

(10) Larentis, S.; Fallahazad, B.; Tutuc, E. Field-effect transistors and intrinsic mobility in ultra-thin $MoSe_2$ layers. *Appl. Phys. Lett.* **2012**, *101*, 223104.

(11) Fang, H.; Tosun, M.; Seol, G.; Chang, T. C.; Takei, K.; Guo, J.; Javey, A. Degenerate n-Doping of Few-Layer Transition Metal Dichalcogenides by Potassium. *Nano Lett.* **2013**, *13*, 1991−1995.

(12) Du, Y.; Liu, H.; Neal, A. T.; Si, M.; Ye, P. D. Molecular Doping of Multilayer MoS_2 Field-Effect Transistors: Reduction in Sheet and Contact Resistances. *IEEE Electron Device Lett.* **2013**, *34*, 1328−1330.

(13) Kiriya, D.; Tosun, M.; Zhao, P.; Kang, J. S.; Javey, A. Air-Stable Surface Charge Transfer Doping of MoS_2 by Benzyl Viologen. *J. Am. Chem. Soc.* **2014**, *136*, 7853−7856.

(14) Yang, L.; Majumdar, K.; Liu, H.; Du, Y.; Wu, H.; Hatzistergos, M.; Hung, P. Y.; Tieckelmann, R.; Tsai, W.; Hobbs, C.; Ye, P. D. Chloride Molecular Doping Technique on 2D Materials: WS_2 and MoS_2. *Nano Lett.* **2014**, *14*, 6275−6280.

(15) Suh, J.; Park, T.-E.; Lin, D.-Y.; Fu, D.; Park, J.; Jung, H. J.; Chen, Y.; Ko, C.; Jang, C.; Sun, Y.; Sinclair, R.; Chang, J.; Tongay, S.; Wu, J. Doping against the Native Propensity of MoS_2: Degenerate Hole Doping by Cation Substitution. *Nano Lett.* **2014**, *14*, 6976−6982.

(16) Gao, J.; Kim, Y. D.; Liang, L.; Idrobo, J. C.; Chow, P.; Tan, J.; Li, B.; Li, L.; Sumpter, B. G.; Lu, T.-M.; Meunier, V.; Hone, J.; Koratkar, N. Transition-Metal Substitution Doping in Synthetic Atomically Thin Semiconductors. *Adv. Mater.* **2016**, *28*, 9735−9743.

(17) Popov, I.; Seifert, G.; Tománek, D. Designing Electrical Contacts to MoS_2 Monolayers: A Computational Study. *Phys. Rev. Lett.* **2012**, *108*, 156802.

(18) Tománek, D. Interfacing graphene and related 2D materials with the 3D world. *J. Phys.: Condens. Matter* **2015**, *27*, 133203.

(19) Zhong, H.; Quhe, R.; Wang, Y.; Ni, Z.; Ye, M.; Song, Z.; Pan, Y.; Yang, J.; Yang, L.; Lei, M.; Shi, J.; Lu, J. Interfacial Properties of Monolayer and Bilayer MoS_2 Contacts with Metals: Beyond the Energy Band Calculations. *Sci. Rep.* **2016**, *6*, 21786.

(20) Wang, Y.; Yang, R. X.; Quhe, R.; Zhong, H.; Cong, L.; Ye, M.; Ni, Z.; Song, Z.; Yang, J.; Shi, J.; Li, J.; Lu, J. Does p-type Ohmic contact exist in WSe_2-metal interfaces? *Nanoscale* **2016**, *8*, 1179−1191.

(21) Kang, J.; Liu, W.; Sarkar, D.; Jena, D.; Banerjee, K. Computational Study of Metal Contacts to Monolayer Transition-Metal Dichalcogenide Semiconductors. *Phys. Rev. X* **2014**, *4*, 031005.

(22) Chen, W.; Santos, E. J. G.; Zhu, W.; Kaxiras, E.; Zhang, Z. Tuning the Electronic and Chemical Properties of Monolayer MoS_2 Adsorbed on Transition Metal Substrates. *Nano Lett.* **2013**, *13*, 509−514.

DOI: 10.1021/acsnano.7b00285
ACS Nano 2017, 11, 3904−3910

(23) Gong, C.; Colombo, L.; Wallace, R. M.; Cho, K. The Unusual Mechanism of Partial Fermi Level Pinning at Metal-MoS_2 Interfaces. *Nano Lett.* **2014**, *14*, 1714−1720.
(24) Movva, H. C. P.; Rai, A.; Kang, S.; Kim, K.; Fallahazad, B.; Taniguchi, T.; Watanabe, K.; Tutuc, E.; Banerjee, S. K. High-Mobility Holes in Dual-Gated WSe_2 Field-Effect Transistors. *ACS Nano* **2015**, *9*, 10402−10410.
(25) Xu, S.; Wu, Z.; Lu, H.; Han, Y.; Long, G.; Chen, X.; Han, T.; Ye, W.; Wu, Y.; Lin, J.; Shen, J.; Cai, Y.; He, Y.; Zhang, F.; Lortz, R.; Cheng, C.; Wang, N. Universal low-temperature Ohmic contacts for quantum transport in transition metal dichalcogenides. *2D Mater.* **2016**, *3*, 021007.
(26) Kappera, R.; Voiry, D.; Yalcin, S. E.; Branch, B.; Gupta, G.; Mohite, A. D.; Chhowalla, M. Phase-engineered low-resistance contacts for ultrathin MoS_2 transistors. *Nat. Mater.* **2014**, *13*, 1128−1134.
(27) Cho, S.; Kim, S.; Kim, J. H.; Zhao, J.; Seok, J.; Keum, D. H.; Baik, J.; Choe, D.-H.; Chang, K. J.; Suenaga, K.; Kim, S. W.; Lee, Y. H.; Yang, H. Phase patterning for Ohmic homojunction contact in $MoTe_2$. *Science* **2015**, *349*, 625−628.
(28) Liu, Y.; Stradins, P.; Wei, S.-H. Van der Waals metal-semiconductor junction: Weak Fermi level pinning enables effective tuning of Schottky barrier. *Sci. Adv.* **2016**, *2*, e1600069.
(29) Chuang, H.-J.; Tan, X.; Ghimire, N. J.; Perera, M. M.; Chamlagain, B.; Cheng, M. M.-C.; Yan, J.; Mandrus, D.; Tománek, D.; Zhou, Z. High Mobility WSe_2 p- and n-Type Field Effect Transistors Contacted by Highly Doped Graphene for Low-Resistance Contacts. *Nano Lett.* **2014**, *14*, 3594−3601.
(30) Du, Y.; Yang, L.; Zhang, J.; Liu, H.; Majumdar, K.; Kirsch, P. D.; Ye, P. D. MoS_2 Field-Effect Transistors With Graphene/Metal Heterocontacts. *IEEE Electron Device Lett.* **2014**, *35*, 599−601.
(31) Liu, Y.; Wu, H.; Cheng, H.-C.; Yang, S.; Zhu, E.; He, Q.; Ding, M.; Li, D.; Guo, J.; Weiss, N. O.; Huang, Y.; Duan, X. Toward Barrier Free Contact to Molybdenum Disulfide Using Graphene Electrodes. *Nano Lett.* **2015**, *15*, 3030−3034.
(32) Yu, Y.-J.; Zhao, Y.; Ryu, S.; Brus, L. E.; Kim, K. S.; Kim, P. Tuning the Graphene Work Function by Electric Field Effect. *Nano Lett.* **2009**, *9*, 3430−3434.
(33) Chuang, H.-J.; Chamlagain, B. P.; Koehler, M.; Perera, M. M.; Yan, J.; Mandrus, D.; Tomanek, D.; Zhou, Z. Low-Resistance 2D/2D Ohmic Contacts: A Universal Approach to High-Performance WSe_2, MoS_2, and $MoSe_2$ Transistors. *Nano Lett.* **2016**, *16*, 1896−1902.
(34) Farmanbar, M.; Brocks, G. Controlling the Schottky barrier at MoS_2/metal contacts by inserting a BN monolayer. *Phys. Rev. B: Condens. Matter Mater. Phys.* **2015**, *91*, 161304.
(35) Das, S.; Gulotty, R.; Sumant, A. V.; Roelofs, A. All Two-Dimensional, Flexible, Transparent, and Thinnest Thin Film Transistor. *Nano Lett.* **2014**, *14*, 2861−2866.
(36) Roy, T.; Tosun, M.; Kang, J. S.; Sachid, A. B.; Desai, S. B.; Hettick, M.; Hu, C. C.; Javey, A. Field-Effect Transistors Built from All Two-Dimensional Material Components. *ACS Nano* **2014**, *8*, 6259−6264.
(37) Cui, X.; Lee, G.-H.; Kim, Y. D.; Arefe, G.; Huang, P. Y.; Lee, C.-H.; Chenet, D. A.; Zhang, X.; Wang, L.; Ye, F.; Pizzocchero, F.; Jessen, B. S.; Watanabe, K.; Taniguchi, T.; Muller, D. A.; Low, T.; Kim, P.; Hone, J. Multi-terminal transport measurements of MoS_2 using a van der Waals heterostructure device platform. *Nat. Nanotechnol.* **2015**, *10*, 534−540.
(38) Marezio, M.; Dernier, P.; Menth, A.; Hull, G. W. The crystal structure of $NbSe_2$ at 15 K. *J. Solid State Chem.* **1972**, *4*, 425−429.
(39) Schutte, W.; De Boer, J. L.; Jellinek, F. Crystal structures of tungsten disulfide and diselenide. *J. Solid State Chem.* **1987**, *70*, 207−209.
(40) Henkelman, G.; Arnaldsson, A.; Jónsson, H. A fast and robust algorithm for Bader decomposition of charge density. *Comput. Mater. Sci.* **2006**, *36*, 354−360.
(41) Sanville, E.; Kenny, S. D.; Smith, R.; Henkelman, G. Improved grid-based algorithm for Bader charge allocation. *J. Comput. Chem.* **2007**, *28*, 899−908.
(42) Tang, W.; Sanville, E.; Henkelman, G. A grid-based Bader analysis algorithm without lattice bias. *J. Phys.: Condens. Matter* **2009**, *21*, 084204.
(43) Yu, M.; Trinkle, D. R. Accurate and efficient algorithm for Bader charge integration. *J. Chem. Phys.* **2011**, *134*, 064111.
(44) Lee, G.-H.; Yu, Y.-J.; Cui, X.; Petrone, N.; Lee, C.-H.; Choi, M. S.; Lee, D.-Y.; Lee, C.; Yoo, W. J.; Watanabe, K.; Taniguchi, T.; Nuckolls, C.; Kim, P.; Hone, J. Flexible and Transparent MoS_2 Field-Effect Transistors on Hexagonal Boron Nitride-Graphene Heterostructures. *ACS Nano* **2013**, *7*, 7931−7936.
(45) Perera, M. M.; Lin, M.-W.; Chuang, H.-J.; Chamlagain, B. P.; Wang, C.; Tan, X.; Cheng, M. M.-C.; Tománek, D.; Zhou, Z. Improved carrier mobility in few-layer MoS_2 field-effect transistors with ionic-liquid gating. *ACS Nano* **2013**, *7*, 4449−4458.
(46) Radisavljevic, B.; Kis, A. Mobility engineering and a metal-insulator transition in monolayer MoS_2. *Nat. Mater.* **2013**, *12*, 815−820.
(47) Chamlagain, B.; Li, Q.; Ghimire, N. J.; Chuang, H.-J.; Perera, M. M.; Tu, H.; Xu, Y.; Pan, M.; Xaio, D.; Yan, J.; Mandrus, D.; Zhou, Z. Mobility Improvement and Temperature Dependence in $MoSe_2$ Field-Effect Transistors on Parylene-C Substrate. *ACS Nano* **2014**, *8*, 5079−5088.
(48) Weck, P. F.; Kim, E.; Czerwinski, K. R. Semiconducting layered technetium dichalcogenides: insights from first-principles. *Dalton Trans.* **2013**, *42*, 15288−15295.
(49) Sata, Y.; Moriya, R.; Masubuchi, S.; Watanabe, K.; Taniguchi, T.; Machida, T. N- and p-type carrier injections into WSe_2 with van der Waals contacts of two-dimensional materials. *Condensed Matter* **2017**, 1.
(50) Kresse, G.; Furthmüller, J. Efficient iterative schemes for *ab initio* total-energy calculations using a plane-wave basis set. *Phys. Rev. B: Condens. Matter Mater. Phys.* **1996**, *54*, 11169−11186.
(51) Kresse, G.; Hafner, J. *Ab initio* molecular dynamics for liquid metals. *Phys. Rev. B: Condens. Matter Mater. Phys.* **1993**, *47*, 558−561.
(52) Kresse, G.; Hafner, J. *Ab initio* molecular-dynamics simulation of the liquid-metal-amorphous-semiconductor transition in germanium. *Phys. Rev. B: Condens. Matter Mater. Phys.* **1994**, *49*, 14251−14269.
(53) Kresse, G.; Joubert, D. From ultrasoft pseudopotentials to the projector augmented-wave method. *Phys. Rev. B: Condens. Matter Mater. Phys.* **1999**, *59*, 1758−1775.
(54) Klimeš, J.; Bowler, D. R.; Michaelides, A. Chemical accuracy for the van der Waals density functional. *J. Phys.: Condens. Matter* **2010**, *22*, 022201.
(55) Klimeš, J.; Bowler, D. R.; Michaelides, A. Van der Waals density functionals applied to solids. *Phys. Rev. B: Condens. Matter Mater. Phys.* **2011**, *83*, 195131.
(56) Monkhorst, H. J.; Pack, J. D. Special points for Brillouin-zone integrations. *Phys. Rev. B: Condens. Matter Mater. Phys.* **1976**, *13*, 5188−5192.
(57) Hestenes, M. R.; Stiefel, E. Methods Of Conjugate Gradients For Solving Linear Systems. *J. Res. Natl. Bur. Stand.* **1952**, *49*, 409−436.

DOI: 10.1021/acsnano.7b00285
ACS Nano 2017, 11, 3904−3910